PHYSICAL REVIEW LETTERS

Articles published week ending 27 MAY 2016

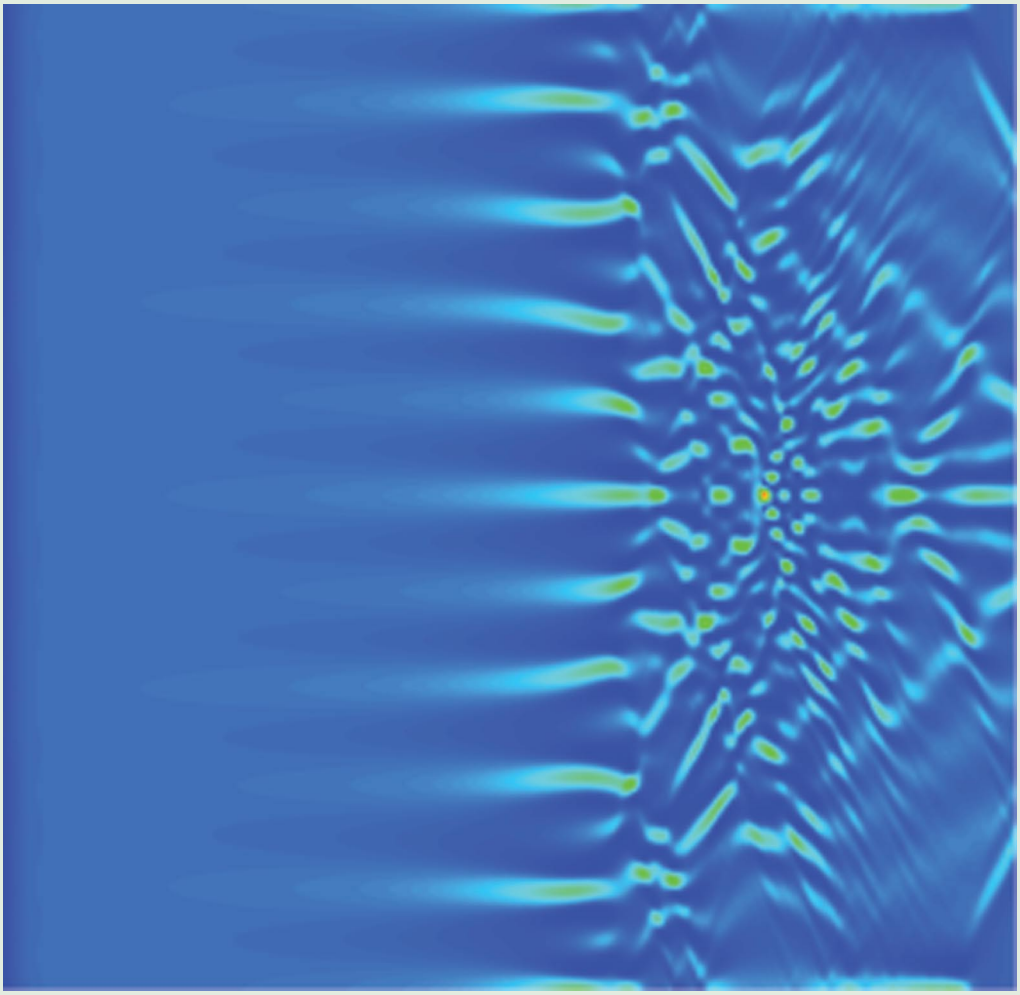

Published by
American Physical Society

APS physics

Volume 116, Number 21

Graphene-Based Active Random Metamaterials for Cavity-Free Lasing

A. Marini[1,*] and F. J. García de Abajo[1,2]
[1]ICFO-Institut de Ciencies Fotoniques, The Barcelona Institute of Science and Technology, 08860 Castelldefels (Barcelona), Spain
[2]ICREA-Institució Catalana de Recerca i Estudis Avançats, Passeig Lluís Companys 23, 08010 Barcelona, Spain
(Received 9 December 2015; published 26 May 2016)

Manipulating and controlling the optical energy flow inside random media is a research frontier of photonics and the basis of novel laser designs. Here, we show that a metamaterial consisting of randomly dispersed graphene nanoflakes embedded within an optically pumped gain medium (rhodamine 6G) can operate as a cavity-free laser thanks to its extraordinarily low threshold for saturable absorption. The emitted light is self-organized into a well-determined spatial pattern, which depends on the graphene flake density and can be externally controlled through the optical pump. We provide different examples of tunable laser operation ranging from stable single-mode to chaoticlike behavior. Our metamaterial design holds great potential for the optical control of light amplification, as well as for the development of single-mode beam-engineered cavity-free lasers.

DOI: 10.1103/PhysRevLett.116.217401

Introduction.—Laser operation is usually achieved through three basic elements: an amplifying medium, an external pumping setup, and an optical cavity that confines and shapes the emitted light in well-determined modes and directions. However, several modern approaches are extending this traditional laser paradigm into new avenues. For instance, the fast developing fiber-laser technology replaces the optical cavity with photonic fibers, thus enabling large average powers and very high beam qualities [1]. Additionally, the advent of nanoplasmonic materials has prompted the demonstration of plasmon stimulated emission in metallic nanoparticles [2–4] and waveguides embedding gaining media [5–8], which enable lasing of surface plasmon polaritons.

In a related context, cavity-free stimulated emission of radiation has been widely studied in random lasers (RLs) [9–11], where the optical cavity modes of traditional lasers are replaced by multiple scattering in disordered media. The complexity underpinning multiple scattering gives rise to several exciting physical phenomena, ranging from Anderson localization of light [12,13] coexisting with extended modes [14,15] to glassy light behavior [16,17] and an interesting interplay with additionally dispersed plasmonic nanoparticles [18,19]. However, RLs lack external tunability, reproducibility, and control over the spatial pattern of the output beam. Overcoming these limitations is central for the development and application of cost-effective cavity-free lasers. In a complementary direction, light amplification has been achieved in artificially engineered materials—metamaterials—that hold promise as planar sources of spatially and temporally coherent radiation [20], for compensating losses in negative-index media [21], and for achieving cavity-free lasing in the stopped-light regime [22,23]. Alternatively, a promising strategy for achieving cavity-free lasing consists in embedding subwavelength random structures in an amplifying medium, so that, rather than undergoing multiple scattering, light experiences the artificially engineered effective optical response of the metamaterial. The extraordinary optical properties of graphene [24–26] are appealing in this context, particularly its highly saturated absorption at rather modest light intensities [27,28], a remarkable feature that has already been exploited for mode-locking in ultrafast fiber lasers [29,30].

In this Letter, we investigate the optical properties of randomly oriented undoped graphene flakes embedded in externally pumped amplifying media (rhodamine 6G). In contrast to traditional RLs, where strong scattering is produced by random inclusions of size commensurate with the light wavelength, here, we focus on the opposite (quasistatic) regime, in which the medium behaves as an active random metamaterial. We demonstrate a novel mechanism leading to stable and tunable single-mode cavity-free lasing: the high nonlinearity of the graphene inclusions produces self-organization of light into peculiar patterns leading to output beams that range from a few to several hundred microns in size. These patterns can be accurately manipulated through both the external pumping setup and the volume density of the graphene flakes, which also enable an interesting transition between chaotic and stable single-mode lasing operation.

Random metamaterial design.—We focus on a disordered medium composed of undoped graphene flakes and rhodamine 6G (R6G) dyes dispersed in polymethylmethacrylate (PMMA), as schematically depicted in Fig. 1(a). We remark that the practical fabrication of such a disordered medium does not involve advanced nanofabrication techniques, as graphene is routinely exfoliated from graphite and dispersed in solutions such as dimethylformamide (DMF), which also dissolves R6G and PMMA. For

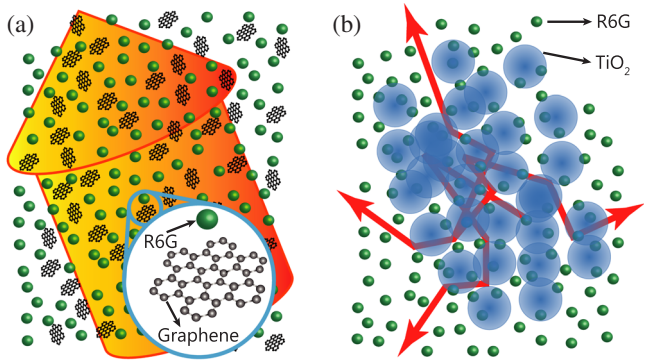

FIG. 1. (a) Our proposed graphene-based active metamaterial consists of a mixture of subwavelength graphene flakes and dispersed rhodamine 6G molecules embedded in PMMA. We envision graphene flakes of 10s nm in size, much smaller than the wavelength of light, which, thus, propagates in an effective medium with an exotic optical response. (b) In contrast, a traditional random laser uses dielectric particles instead of graphene, with sizes and separations that are comparable with the light wavelength in order to efficiently produce multiple scattering.

simplicity, we assume the graphene flakes to be disks with volume density N and diameter $D = 30$ nm, for which quantum many-body and finite-size effects are negligible [31]. We emphasize that unintentional doping of the flakes ($E_F \approx 0.2$ eV), their geometric details, and their specific size do not significantly influence their optical response in the visible regime (geometry- and size-dependent resonances appear at infrared and lower frequencies under such low doping). As we show below [see Supplemental Material (SM) [32] as well], the effective optical response of the random medium only depends on the graphene filling fraction $f = N\pi(D/2)^2 a$, where $a = 0.335$ nm is an effective thickness taken from the interlayer distance in graphite.

R6G constitutes the optically amplifying medium, in which population inversion can be achieved through a frequency-doubled Nd-YAG laser-pump beam at wavelength $\lambda = 532$ nm. The aimed wavelength of laser operation is $\lambda = 593$ nm, where R6G has its peak emission. Under these conditions, graphene flakes are much smaller than the optical wavelength and scattering is quite inefficient, so that their effect on optical propagation is captured by the effective permittivity of the composite material (see below). To place this in context, typical RLs also work with R6G dispersed in PMMA [33], but in contrast, multiple scattering is efficiently achieved through randomly positioned particles whose dimensions are comparable with the optical wavelength [see Fig. 1(b)].

Saturable absorption of graphene.—In order to obtain the effective permittivity of our metamaterial, we first need to understand how the response of the graphene flakes varies under the effect of a strong optical field. The conical band structure of undoped graphene around the Dirac points [see Fig. 2(a)] is responsible for its unique properties. Valence electrons in this material behave as two-dimensional massless Dirac fermions with constant Fermi velocity $v_F \simeq 10^6$ m/s [34,35]. As a consequence, graphene exhibits a broadband nearly constant absorbance $\alpha_0 \approx \pi/137$ in the limit of small excitation intensities [36,37], which also reflects a dispersionless linear conductivity $\sigma_0 = e^2/(4\hbar)$. However, at higher light intensities, absorption saturates due to the nonlinear dynamics of graphene electrons [see Fig. 2(a)]. In simple terms, in the strong-field regime, electron-hole recombination produced by electron collisions can balance light-induced interband absorption, which is, in turn, partially inhibited by Pauli blocking of out-of-equilibrium electrons in the conduction band [see Fig. 2(a)]. In most materials, this leads to a light-intensity (I) dependence of the absorbance α, which typically follows a law $\alpha(I) = \alpha_0/[1 + I/I_S]$, where I_S is the saturation intensity. However, we find that the peculiar band structure of graphene produces a different intensity dependence of the absorbance: $\alpha(I) = \alpha_0/\sqrt{1 + I/I_S}$, where $I_S = 137\pi\hbar\omega_S^2 c^2/(2v_F^2\lambda^2)$ and $\omega_S = 6.16$ rad ps^{-1} (see details in the SM [32]). Interestingly, we find a remarkably small value of $I_S \simeq 22$ MW/cm^2 (at $\lambda = 593$ nm), which is consistent with experimental findings [27,28]. In brief, we model out-of-equilibrium electron dynamics through graphene Bloch equations [38,39], which we solve numerically in the presence of an external monochromatic electric field $\mathbf{E}(t) = \mathrm{Re}[E_0 e^{-i\omega t}]\hat{x}$ with angular frequency ω and polarization along the $\hat{x}$ direction (see details in the SM [32]). Electron-hole recombination processes are taken into account through a decay time τ, which, in our calculations, is assumed to be $\tau = 100$ fs. This phenomenological parameter accounts for the different and involved ultrafast

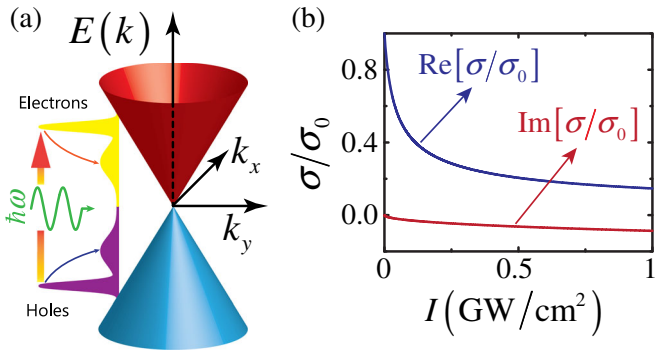

FIG. 2. (a) Conical band structure around the Dirac points. Upper $E_+(k) = +\hbar v_F k$ and lower $E_-(k) = -\hbar v_F k$ energy bands depend linearly on the electron wave vector k. Interband transitions produced by impinging photons with energy $\hbar\omega$ lead to an out-of-equilibrium electron distribution, which then relaxes via electron collisions. After an initial transient time, optical pumping and electron relaxation compensate each other, and absorption is saturated due to partial Pauli blocking. (b) Intensity-dependent conductivity $\sigma(I)$ (which is frequency independent) normalized to the universal conductivity $\sigma_0 = e^2/4\hbar$.

decay channels of out-of-equilibrium electrons into hot carriers and phonons [40–42], which are treated in the relaxation approximation. We numerically solve the Bloch equations neglecting higher harmonic terms and calculating the macroscopic current density $\mathbf{J}(t)$ [32,38,39]. The intensity-dependent conductivity $\sigma(I)$, which is plotted in Fig. 2(b), is straightforwardly extracted from $\mathbf{J} = \mathrm{Re}[\sigma \mathbf{E}]$.

Averaged optical response.—We model R6G amplification through the traditional Bloch description of two-level systems, where the external optical pumping is assumed to yield a stable population inversion. For monochromatic waves, Bloch dynamics can be solved analytically and, at resonance, reduce to a purely imaginary susceptibility accounting for gain: $\chi_{\mathrm{R6G}} = -i(g_0/k_0)/[1 + I/I_S^{\mathrm{R6G}}]$, where $k_0 = 2\pi/\lambda$ is the vacuum wave vector, $\lambda =$ 593 nm (see above), g_0 is the unsaturated gain coefficient (which depends on R6G density and can be tuned through the external pump at $\lambda_{\mathrm{pump}} = 532$ nm), and $I_S^{\mathrm{R6G}} \simeq$ 150 MW/cm^2 is the R6G saturation intensity [43]. For simplicity, we disregard the effect of the optical pump on graphene flakes. We note that unsaturated gain values of about $g_0 \simeq 400$ cm^{-1} have been experimentally demonstrated with R6G [5]. PMMA contributes to the optical response through a background dielectric constant $\epsilon_b \simeq$ 2.23 at the operating wavelength. Randomly oriented graphene disks are modeled through a standard quasistatic approach [26,32]. The optical response of undoped graphene disks is thoroughly accounted for by the first dipolar resonance tail, which gives the polarizability $\alpha_G = D^3/\{3/(2\epsilon_b) - 8i\epsilon_0 cD/[\lambda\sigma(I)]\} \simeq \pi(D/2)^2 a\chi_G$, where $\chi_G = i\sigma(I)/(a\epsilon_0\omega)$. The total response of the system is finally calculated through Clausius-Mossotti effective-medium theory in the limit of small graphene density: $\epsilon_{\mathrm{eff}}(I) \simeq \epsilon_b + \chi_{\mathrm{R6G}} + (2/3) f\chi_G$, where the factor 2/3 accounts for averaging over the random orientation of the disks (see SM [32] for more details). The optical properties of the random medium, including PMMA, saturated R6G amplification, graphene absorption, and the induced phase shift, are thus fully contained within $\epsilon_{\mathrm{eff}}(I)$. We emphasize that in the regime considered here, the effective response $\epsilon_{\mathrm{eff}}(I)$ does not depend on the size or shape of the graphene flakes but only on their filling fraction $f = N\pi(D/2)^2 a$.

Dissipative optical dynamics.—Now, we use the above results to simulate light amplification and lasing under specific pumping conditions, describing self-organization mechanisms of seed light beams launched inside the bulk medium [see Fig. 3(a)]. Nonlinear propagation in the effective medium under consideration is modeled through the slowly varying envelope approach [32,44], where the seed optical field is expressed as $\mathbf{E}(\mathbf{r}, t) = A(\mathbf{r}_\perp, z)e^{ik_0(\sqrt{\epsilon_b}z - ct)}\mathbf{n}$, $\mathbf{r} = (\mathbf{r}_\perp, z)$ is the position vector, $\mathbf{n}$ is a unit vector accounting for the arbitrary linear polarization of the beam, and the optical envelope $A(z, \mathbf{r}_\perp)$ is governed by

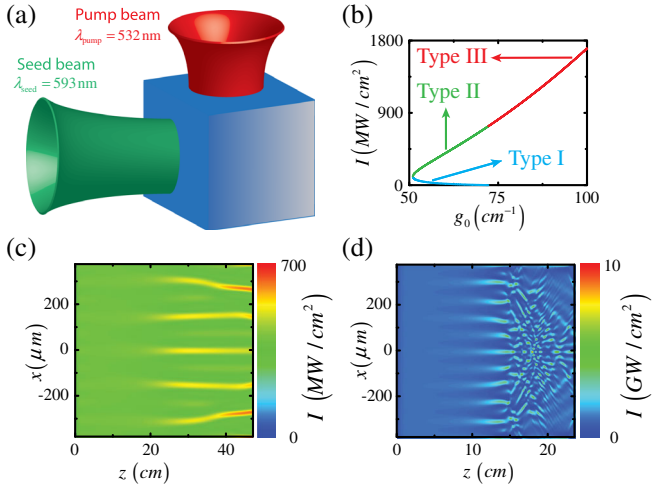

FIG. 3. (a) Schematic of the system excitation: a pump beam produces inversion of population that provides an effective gain coefficient g_0, while a seed beam launched in the disordered bulk undergoes amplification through stimulated emission. (b) Existence curve of extended modes, showing their intensity $I = (1/2)\epsilon_0 c|A_0|^2$ against the gain coefficient g_0. (c),(d) Propagation of perturbed extended modes: (c) type II for $g_0 = 60$ cm^{-1} and (d) type III for $g_0 = 85$ cm^{-1}. Graphene flakes are assumed to be disks of diameter $D = 30$ nm and density $N = 10^3$ μm^{-3}.

$$2ik_0\sqrt{\epsilon_b}\partial_z A + \nabla_\perp^2 A + k_0^2[\epsilon_{\mathrm{eff}}(|A|^2) - \epsilon_b]A = 0, \quad (1)$$

(see SM [32] for further details). Extended homogeneous nonlinear modes can be excited by launching a seed extended plane wave, and are calculated by setting the ansatz $A(z) = A_0 e^{i\beta z}$ in Eq. (1), where $\beta = (k_0/2\sqrt{\epsilon_b})\{\mathrm{Re}[\epsilon_{\mathrm{eff}}(|A_0|^2)] - \epsilon_b\}$ is the propagation constant correction, while the mode amplitude A_0 is fixed by the condition $\mathrm{Im}[\epsilon_{\mathrm{eff}}(|A_0|^2)] = 0$. We solve Eq. (1) using the Newton-Raphson method for several values of the gain coefficent g_0 [see Fig. 3(b)]. We find three types of extended nonlinear modes departing from the trivial solution $A_0 = 0$: Types I and II coexist in the bistable subcritical domain, while type III exists only in the overcritical domain [see Fig. 3(b), where subcritical or overcritical domains are separated by the threshold gain coefficient $g_0 \approx$ 72 cm^{-1}]. We further evaluate the stability properties of these modes, finding that every extended mode is modulationally unstable [32]. In addition, type II (III) extended modes exist on top of a stable (unstable) background $A_0 = 0$. Thus, nonlinear dynamics in subcritical or overcritical domains leads to qualitatively different phenomena [see Figs. 3(c) and 3(d)].

Discussion.—These results prelude the existence of localized nonlinear modes with complex patterns indicating that, under extended seed excitation, unstable homogeneous modes dynamically evolve into either (i) a series of stable filaments for subcritical gain values [see Fig. 3(c)]

or (ii) a chaoticlike spatial dynamics of unstable filaments for overcritical gain values [see Fig. 3(d)]. In the context of dissipative systems, these kinds of localized nonlinear modes are commonly named dissipative solitons (DSs) [45], as they involve an internal power flow enabling stationary propagation. We further investigate the properties of these $(1+1)$D light beams by setting the ansatz $A(x,z) = A_0(x)e^{i\beta z}$ in Eq. (1). The ensuing differential equation for $A_0(x)$ is again solved numerically, finding a set of bell-shaped DSs [32]. Analogous to extended modes, we identify three types of localized nonlinear modes: DS1 and DS2 coexist in the bistable subcritical domain, while DS3 exists only in the overcritical domain [see Fig. 4(a), where we plot their maximum intensity $I_{\max} = (1/2)\epsilon_0 c \max|A_0(x)|^2$ and their width w against g_0 for fixed graphene flake density $N = 10^3\ \mu\text{m}^{-3}$]. We emphasize that the mode patterns are complex, so that, for every localized mode, there is a peculiar internal power flow enabling stationary propagation within an intensity-dependent absorption or amplification environment [32]. We analyze mode stability over propagation by solving Eq. (1) through the split-step fast-Fourier-transform method embedding a fourth-order Runge Kutta routine, finding that only DS2 modes are stable. In view of the stability features of extended and localized modes, we note that there exists only one single stable mode (DS2) for every fixed value of g_0 and N within the subcritical domain. The spatial size and peak intensity of this unique bell-shaped stable mode is fixed by g_0 and N [see Fig. 4(a)]. Consequently, the mode features can be externally manipulated by tuning the optical pump or the graphene flake density [see Fig. 4(b), where we plot the mode minimum width $w_{\min}$ and the corresponding g_0 as a function of N]. Note that the single-mode spatial width can be tuned from a few tenths to several hundreds of microns, while its spectral width is fixed by the resonant gaining medium (for R6G used in our calculations the mode spectral width is about 2 meV [33]). Excitation with an extended seed leads to a collection of interacting filaments [see Fig. 3(c)]. In contrast, the single-mode regime emerges when the system is excited by a localized Gaussian seed, which directly fixes the direction of propagation. In Figs. 4(c) and 4(d), we plot the propagation of an input Gaussian seed $I(x) = I_0 e^{-(x/w)^2}$ with peak intensity $I_0 = 70\ \text{MW/cm}^2$ and width $w = 70\ \mu\text{m}$ for a fixed gain coefficient $g_0 = 55\ \text{cm}^{-1}$ and for two different graphene flake densities: Fig. 4(c) $N = 1000\ \mu\text{m}^{-3}$ and Fig. 4(d) $N = 900\ \mu\text{m}^{-3}$. Interestingly, by manipulating N, one can tune the system from seed amplification into a stable single mode [Fig. 4(c)] to chaotic dynamics [Fig. 4(d)].

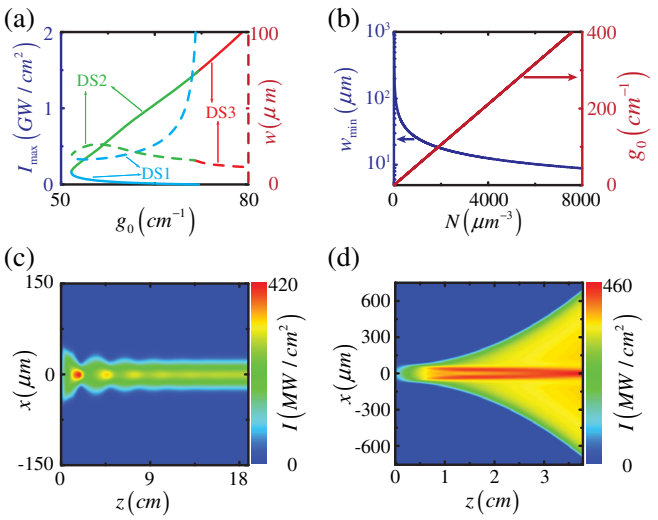

FIG. 4. (a) Existence domain of DS1, DS2, and DS3 localized modes (cyan, green, and red curves) showing their maximum intensity $I_{\max}$ (left, blue axis, full curves) and width w (right, red axis, dashed curves) against the gain coefficient g_0 ($N = 10^3\ \mu\text{m}^{-3}$). (b) DS2 minimum width $w_{\min}$ (red curve) and corresponding gain coefficient g_0 (blue curve) plotted against the graphene flake density N. (c),(d) Propagation of an input Gaussian seed $I(x) = I_0 e^{-(x/w)^2}$ with peak intensity $I_0 = 70\ \text{MW/cm}^2$ and width $w = 70\ \mu\text{m}$ naturally evolving into (c) the stable DS2 mode with width $w \simeq 30\ \mu\text{m}$ and peak intensity $I_{\max} \simeq 0.3\ \text{GW/cm}^2$ and (d) unstable chaotic dynamics [$g_0 = 55\,\text{cm}^{-1}$ with (c) $N = 1000\ \mu\text{m}^{-3}$ and (d) $N = 900\ \mu\text{m}^{-3}$].

This leads to the conclusion that the graphene-based active random metamaterials under discussion enable single-mode operation with spatial patterns determined by the external optical pump (which tunes the gain coefficient g_0) and the density of graphene flakes. Our results are based on realistic physical parameters of the materials adopted and indicate that single-mode cavity-free lasing can be achieved at the micrometer scale with current technology.

Conclusion.—In summary, the extremely low-threshold saturable absorption of graphene allows us to design an active random metamaterial capable of sustaining single-mode size- or shape-controlled laser beams. The external pump intensity and the density of graphene flakes determine the regime of operation, which can be varied from chaotic to stable single mode. Because the proposed random medium is a disordered mixture of currently available materials, it is promising as an inexpensive and versatile platform for the design of cavity-free light amplifiers and lasers.

This work has been partially supported by the Spanish MINECO (Grants No. MAT2014-59096-P and No. SEV-2015-0522) and the European Commission (Graphene Flagship Grants No. CNECT-ICT-604391 and No. FP7-ICT-2013-613024-GRASP). A. M. is supported by an ICFOnest + Postdoctoral Fellowship (Marie Curie COFUND program). We acknowledge useful discussions with Joel Cox and Valerio Pruneri.

*andrea.marini@icfo.es

[1] C. Jauregui, J. Limpert, and A. Tünnermann, Nat. Photonics **7**, 861 (2013).
[2] D. J. Bergman and M. I. Stockman, Phys. Rev. Lett. **90**, 027402 (2003).
[3] M. A. Noginov, G. Zhu, A. M. Belgrave, R. Bakker, V. M. Shalaev, E. E. Narimanov, S. Stout, E. Herz, T. Suteewong, and U. Wiesner, Nature (London) **460**, 1110 (2009).
[4] M. I. Stockman, J. Opt. **12**, 024004 (2010).
[5] M. A. Noginov, G. Zhu, M. Mayy, B. A. Ritzo, N. Noginova, and V. A. Podolskiy, Phys. Rev. Lett. **101**, 226806 (2008).
[6] A. Marini, A. V. Gorbach, D. V. Skryabin, and A. V. Zayats, Opt. Lett. **34**, 2864 (2009).
[7] P. M. Bolger, W. Dickson, A. V. Krasavin, L. Liebscher, S. G. Hickey, D. V. Skryabin, and A. V. Zayats, Opt. Lett. **35**, 1197 (2010).
[8] I. De Leon and P. Berini, Nat. Photonics **4**, 382 (2010).
[9] D. S. Wiersma, Nat. Phys. **4**, 359 (2008).
[10] S. Gottardo, R. Sapienza, P. D. García, A. Blanco, D. S. Wiersma, and C. López, Nat. Photonics **2**, 429 (2008).
[11] D. S. Wiersma, Nat. Photonics **7**, 188 (2013).
[12] P. Sebbah and C. Vanneste, Phys. Rev. B **66**, 144202 (2002).
[13] M. Segev, Y. Silberberg, and D. N. Christodoulides, Nat. Photonics **7**, 197 (2013).
[14] S. Mujumdar, M. Ricci, R. Torre, and D. S. Wiersma, Phys. Rev. Lett. **93**, 053903 (2004).
[15] J. Fallert, R. J. B. Dietz, J. Sartor, D. Schneider, C. Klingshirn, and H. Kalt, Nat. Photonics **3**, 279 (2009).
[16] L. Angelani, C. Conti, G. Ruocco, and F. Zamponi, Phys. Rev. Lett. **96**, 065702 (2006).
[17] N. Ghofraniha, I. Viola, F. Di Maria, G. Barbarella, G. Gigli, L. Leuzzi, and C. Conti, Nat. Commun. **6**, 6058 (2015).
[18] X. Meng, K. Fujita, S. Murai, T. Matoba, and K. Tanaka, Nano Lett. **11**, 1374 (2011).
[19] X. Meng, K. Fujita, Y. Zong, S. Murai, and K. Tanaka, Appl. Phys. Lett. **92**, 201112 (2008).
[20] N. I. Zheludev, S. L. Prosvirnin, N. Papasimakis, and V. A. Fedotov, Nat. Photonics **2**, 351 (2008).
[21] S. Wuestner, A. Pusch, K. L. Tsakmakidis, J. M. Hamm, and O. Hess, Phys. Rev. Lett. **105**, 127401 (2010).
[22] O. Hess, J. B. Pendry, S. A. Maier, R. F. Oulton, J. M. Hamm, and K. L. Tsakmakidis, Nat. Mater. **11**, 573 (2012).
[23] A. Marini and F. J. García de Abajo, Sci. Rep. **6**, 20088 (2016).
[24] F. Bonaccorso, Z. Sun, T. Hasan, and A. C. Ferrari, Nat. Photonics **4**, 611 (2010).
[25] Q. Bao and K. P. Loh, ACS Nano **6**, 3677 (2012).
[26] F. J. García de Abajo, ACS Photonics **1**, 135 (2014).
[27] Q. Bao, H. Zhang, Y. Wang, Z. Ni, Y. Yan, Z. X. Shen, K. P. Loh, and D. Y. Tang, Adv. Funct. Mater. **19**, 3077 (2009).
[28] G. Xing, H. Guo, X. Zhang, T. C. Sum, and C. H. A. Huan, Opt. Express **18**, 4564 (2010).
[29] Z. Sun, T. Hasan, F. Torrisi, D. Popa, G. Privitera, F. Wang, F. Bonaccorso, D. M. Basko, and A. C. Ferrari, ACS Nano **4**, 803 (2010).
[30] A. Martinez and Z. Sun, Nat. Photonics **7**, 842 (2013).
[31] J. D. Cox and F. J. García de Abajo, Nat. Commun. **5**, 5725 (2014).
[32] See Supplemental Material at http://link.aps.org/supplemental/10.1103/PhysRevLett.116.217401 for more details on the technical aspects of the theory.
[33] M. Leonetti, C. Conti, and C. Lopez, Nat. Commun. **4**, 1740 (2013).
[34] K. S. Novoselov, A. K. Geim, S. V. Morozov, D. Jiang, Y. Zhang, S. V. Dubonos, I. V. Grigorieva, and A. A. Firsov, Science **306**, 666 (2004).
[35] K. S. Novoselov, A. K. Geim, S. V. Morozov, D. Jiang, M. I. Katsnelson, I. V. Grigorieva, S. V. Dubonos, and A. A. Firsov, Nature (London) **438**, 197 (2005).
[36] R. R. Nair, P. Blake, A. N. Grigorenko, K. S. Novoselov, T. J. Booth, T. Stauber, N. M. R. Peres, and A. K. Geim, Science **320**, 1308 (2008).
[37] K. F. Mak, M. Y. Sfeir, Y. Wu, C. H. Lui, J. A. Misewich, and T. F. Heinz, Phys. Rev. Lett. **101**, 196405 (2008).
[38] K. L. Ishikawa, Phys. Rev. B **82**, 201402(R) (2010).
[39] K. L. Ishikawa, New J. Phys. **15**, 055021 (2013).
[40] J. C. Johannsen *et al.*, Phys. Rev. Lett. **111**, 027403 (2013).
[41] I. Gierz, J. C. Petersen, M. Mitrano, C. Cacho, I. C. E. Turcu, E. Springate, A. Stöhr, A. Köhler, U. Starke, and A. Cavalleri, Nat. Mater. **12**, 1119 (2013).
[42] D. Brida *et al.*, Nat. Commun. **4**, 1987 (2013).
[43] B. Nithyaja, H. Misha, P. Radhakrishnan, and V. P. N. Nampoor, J. Appl. Phys. **109**, 023110 (2011).
[44] M. Leonetti, C. Conti, and C. Lopez, Light Sci. Appl. **2**, e88 (2013).
[45] P. Grelu and N. Akhmediev, Nat. Photonics **6**, 84 (2012).

Graphene-Based Active Random Metamaterials for Cavity-Free Lasing - SUPPLEMENTARY MATERIAL -

A. Marini[1,*] and F. J. García de Abajo[1,2]
[1] *ICFO-Institut de Ciencies Fotoniques, The Barcelona Institute of Science and Technology, 08860 Castelldefels (Barcelona), Spain and*
[2] *ICREA-Institució Catalana de Recerca i Estudis Avançats, Barcelona, Spain*
(Dated: May 19, 2016)

We provide additional information on graphene saturable absorption, the amplification properties of the active medium (Rhodamine 6G), and the composite effective response, as well as homogeneous and localized dissipative modes and their stability. Additionally, we give details on our theoretical derivations and computational methods.

I. SATURABLE ABSORPTION OF GRAPHENE

We model light-induced out-of-equilibrium dynamics of two-dimensional massless Dirac fermions (MDFs) through generalized Bloch equations (GBEs), which can be directly derived from the 2D Dirac equation for MDFs with momentum $\mathbf{p}$ [1, 2]. In this approach, MDFs are let to interact with an external monochromatic electric field $\mathbf{E}(t) = \mathrm{Re}\left[E_0 e^{-i\omega t}\right]\hat{x}$ with angular frequency ω and polarization along the $\hat{x}$ direction. The electromagnetic interaction is introduced through the minimal coupling $\boldsymbol{\pi}(t) = \mathbf{p} + e\mathbf{A}(t)$, where the MDF quasi-momentum $\boldsymbol{\pi}(t)$ is temporally driven by the potential vector $\mathbf{A}(t) = -\int \mathbf{E}(t')dt'$. The temporal dynamics of the $\mathbf{p}$-dependent coherence $\Gamma_{\mathbf{p}}(t)$ and inversion of population $n_{\mathbf{p}}(t)$ is governed by GBEs, which in the $eA(t) << \hbar\omega/v_{\mathrm{F}}$ limit are explicitly given by

$$\dot{\Gamma}_{\mathbf{p}} = -\left(\frac{1}{T_2} + i\omega_0\right)\Gamma_{\mathbf{p}} - \frac{ie}{2p}\mathrm{Re}\left[E_0 e^{-i\omega t}\right]\sin\varphi n_{\mathbf{p}}, \tag{1}$$

$$\dot{n}_{\mathbf{p}} = -\frac{1}{T_1}\left(n_{\mathbf{p}} + 1\right) + \frac{2e}{p}\mathrm{Re}\left[E_0 e^{-i\omega t}\right]\sin\varphi \mathrm{Im}\Gamma_{\mathbf{p}}, \tag{2}$$

where $\omega_0 = 2v_{\mathrm{F}}p/\hbar$, and the electron momentum is expressed in polar coordinates $\mathbf{p} = p(\cos\varphi, \sin\varphi)$. Electron-hole recombination processes are taken into account through the phenomelogical parameters T_1, T_2, which represent the population decay and the coherence dephasing time-scales, respectively. In our calculations we assume $T_1 = T_2 =$ 100fs. We obtain steady-state analytical solutions of Eqs. (1-2) by using the ansatz

$$\Gamma_{\mathbf{p}} = \Gamma^{+}_{\mathbf{p}} e^{i\omega t} + \Gamma^{-}_{\mathbf{p}} e^{-i\omega t},$$
$$n_{\mathbf{p}} = n^{0}_{\mathbf{p}} + \mathrm{Re}\left[n^{\Omega}_{\mathbf{p}} e^{-2i\omega t}\right],$$

and solving the ensuing system of algebraic equations for $\Gamma^{\pm}_{\mathbf{p}}, n^{0}_{\mathbf{p}}$, and $n^{\Omega}_{\mathbf{p}}$ neglecting third-harmonic terms. In the limit of vanishing Fermi energy and temperature, the total current density induced on the graphene is given by

$$\mathbf{J}(t) = 2ev_{\mathrm{F}}\frac{g_{\mathrm{s}}g_{\mathrm{v}}}{(2\pi\hbar)^2}\hat{x}\int_0^{2\pi}\sin\varphi d\varphi\int_0^{\infty} p\Gamma_{\mathbf{p}}(t)dp,$$

where $g_{\mathrm{s}} = 2$ and $g_{\mathrm{v}} = 2$ are the spin and valley degeneracy factors. The graphene conductivity σ is thus straightforwardly extracted from $\mathbf{J} = \mathrm{Re}[\sigma\mathbf{E}]$. We have numerically solved the above integrals for several light intensities $I = (1/2)\epsilon_0 c|E_0|^2$, and found good fitting with the following analytical expression for $\sigma(I)$:

$$\sigma(I) = \sigma_0\left[\frac{1}{\sqrt{1 + I/I_{\mathrm{S}}}} - i\frac{1 - e^{-\eta_1\sqrt{I/I_{\mathrm{S}}}}}{\sqrt{1 + \eta_2(I/I_{\mathrm{S}})^{0.4}}}\right],$$

where $\sigma_0 = e^2/(4\hbar)$, $I_{\mathrm{S}} = 137\hbar\omega_{\mathrm{S}}^2\omega^2/(8\pi v_{\mathrm{F}}^2)$, $\omega_{\mathrm{S}} = 6.16$ rad ps^{-1}, $\eta_1 = (\omega_\eta/\omega)$, $\eta_2 = (\omega_\eta/\omega)^{0.8}$, and $\omega_\eta = 46.20$ rad ps^{-1}.

*Electronic address: andrea.marini@icfo.es

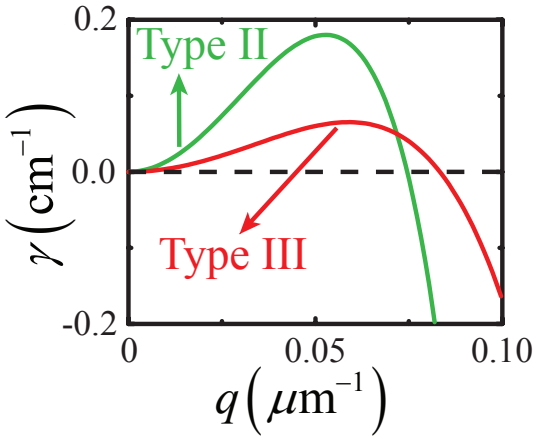

FIG. S1: Gain spectrum illustrating the instability growth coefficient γ against the small-amplitude perturbation wave-vector q for type II ($g_0 = 60$ cm^{-1}) and III ($g_0 = 85$ cm^{-1}) modes. The instability occurs when $\gamma > 0$. Graphene flakes are assumed to be disks of diameter $D = 30$ nm and density $N = 10^3$ μm^{-3}.

II. AMPLIFICATION OF THE ACTIVE MEDIUM

We consider externally pumped R6G as the gain medium. The optical response of R6G is modeled through the traditional Bloch equations (BEs) of two-level systems with resonant angular frequency $\omega_{\rm ba}$ and transition dipole moment $\mu_{\rm ba}$. The temporal dynamics of the density matrix coherence $\rho_{\rm ba} = r_{\rm ba}e^{-i\omega t}$ and population inversion $n_{\rm ba} = \rho_{\rm bb} - \rho_{\rm aa}$ under the external monochromatic driving field is governed by the BEs

$$\dot{r}_{\rm ba} = i(\omega - \omega_{\rm ba})r_{\rm ba} - \frac{1}{\tau_2}r_{\rm ba} - \frac{i}{\hbar}\mu_{\rm ba}E_0 n_{\rm ba},$$
$$\dot{n}_{\rm ba} = \frac{1}{\tau_1}\left[n_{\rm ba}^{\rm eq} - n_{\rm ba}\right] - \frac{4}{\hbar}{\rm Im}\left[\mu_{ba}E_0 r_{\rm ba}^*\right],$$

where $n_{\rm ba}^{\rm eq} > 0$ is the equilibrium population inversion induced by the external pump, τ_1 and τ_2 are the characteristic population decay and coherence dephasing times of R6G, respectively, and we adopt the rotating wave approximation. Furthermore, we assume that R6G is operating at resonance (i.e., $\omega = \omega_{\rm ba}$). Stationary solutions of the BEs are thus directly found by setting $\dot{r}_{\rm ba} = \dot{n}_{\rm ba} = 0$. The R6G induced polarization is in turn given by $\mathbf{P}(t) = N_{\rm R6G}(\mu_{\rm ba}^*\rho_{\rm ba} + \mu_{\rm ba}\rho_{\rm ba}^*)$, where $N_{\rm R6G}$ is the R6G density. Hence, the R6G susceptibility becomes

$$\chi_{\rm R6G} = -i\frac{(g_0/k)}{1 + I/I_{\rm S}^{\rm R6G}},$$

where $I_{\rm S}^{\rm R6G} \simeq 150$ MW/cm^2 is the R6G saturation intensity [3]. The gain coefficient g_0 depends linearly on the equilibrium population inversion $n_{\rm ba}^{\rm eq}$, so that it can be controlled through the external pump and can reach values as large as $g_0 \simeq 400$ cm^{-1} [4].

III. AVERAGED OPTICAL RESPONSE OF THE DISORDERED MIXTURE

The optical response of the system depends on its three underpinning constituents: embedding PMMA, externally-pumped R6G, and randomly-oriented subwavelength graphene disks of diameter $D = 30$ nm. Graphene is routinely exfoliated from graphite and dispersed in several solutions including dimethylformamide (DMF), which can also be used to dissolve R6G and PMMA. We emphasize that the practical fabrication of such a disordered medium does not involve advanced nano-fabrication techniques. PMMA contributes to the optical response with a background dielectric constant $\epsilon_{\rm b} \simeq 2.23$ at the operating wavelength. The polarizability of subwavelength randomly-oriented graphene disks is calculated through a standard electrostatic approach [5], considering only the first dipolar resonance tail:

$$\alpha_{\rm G} = \frac{D^3}{3/(2\epsilon_{\rm b}) - 8i\epsilon_0 cD/[\lambda\sigma(I)]},$$

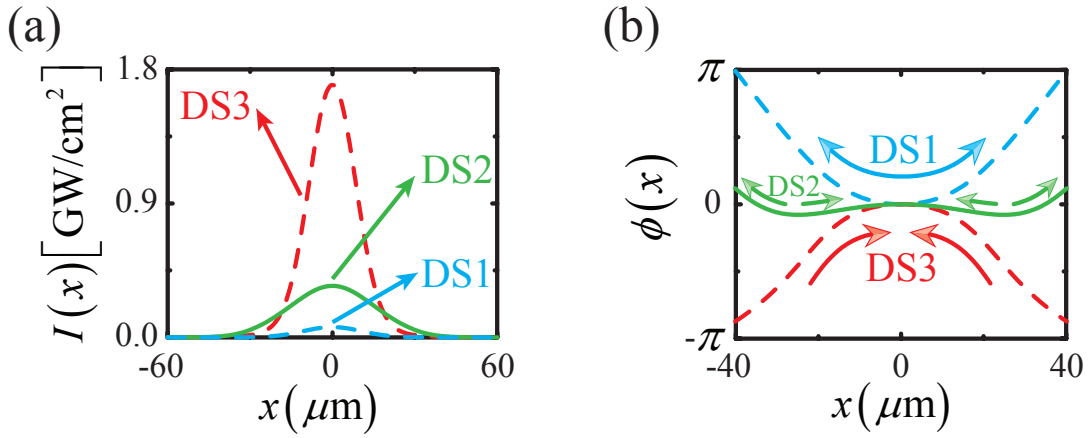

FIG. S2: **Localized lasing modes**. Three localized mode types are identified: DS1 and DS2 coexist in the sub-critical domain, while only DS3 exists in the over-critical domain. **(a)** Intensity $I(x)$ and **(b)** transverse phase $\phi(x)$ profiles for the three different localized mode types: DS1, DS2 ($g_0 = 55$ cm^{-1}), and DS3 ($g_0 = 75$ cm^{-1}). Arrows in **(b)** indicate the transverse power flow of each mode. Graphene flakes are assumed to be disks of diameter $D = 30$ nm and density $N = 10^3$ μm^{-3}.

which is well approximated by $\alpha_{\mathrm{G}} \simeq \pi(D/2)^2 a\chi_{\mathrm{G}}$, where $\chi_{\mathrm{G}} = i\sigma(I)/(a\epsilon_0\omega)$, since graphene plasmons do not come into play at the optical frequencies considered here. The total response of the system is thus calculated through the Clausius-Mossotti effective response theory

$$\frac{\epsilon_{\mathrm{eff}} - \epsilon_{\mathrm{ext}}}{\epsilon_{\mathrm{eff}} + 2\epsilon_{\mathrm{ext}}} = \frac{(2/3)N\alpha_{\mathrm{G}}}{3\epsilon_{\mathrm{ext}}},$$

where the factor 2/3 accounts for the random orientation of graphene disks and $\epsilon_{\mathrm{ext}} = \epsilon_{\mathrm{b}} + \chi_{\mathrm{R6G}}$. In the limit of small graphene density, the Clausius-Mossotti expression reduces to $\epsilon_{\mathrm{eff}}(I) \simeq \epsilon_{\mathrm{b}} + \chi_{\mathrm{R6G}} + (2/3)f\chi_{\mathrm{G}}$.

IV. NONLINEAR DISSIPATIVE DYNAMICS

Optical propagation of monochromatic waves inside the disordered amplifying medium is ruled by the double-curl macroscopic Maxwell's equations with nonlinear effective constant $\epsilon_{\mathrm{eff}}(I)$:

$$\nabla \times \nabla \times \mathbf{E} = k_0^2 \epsilon_{\mathrm{eff}}(I)\mathbf{E}.$$

By taking the ansatz $\mathbf{E}(\mathbf{r}, t) = A(\mathbf{r}_\perp, z)e^{ik_0(\sqrt{\epsilon_{\mathrm{b}}}z - ct)}\hat{n}$, where $\hat{n}$ is the arbitrary polarization unit vector, and adopting the slowly varying envelope approach (SVEA) $|\partial_z A| << k\sqrt{\epsilon_{\mathrm{b}}}|A|$, $\nabla \cdot \mathbf{E} \simeq 0$, we can neglect second-order derivatives of the envelope $\partial_z^2 A$, leading to Eq. (1) of the main paper. The SVEA ceases to be valid for optical beams with size comparable to the wavelength, in which case the longitudinal component of the field becomes relevant. However, we never approach this limit in our calculations, and the SVEA remains fully valid for the results presented here.

Extended homogeneous nonlinear modes are calculated by setting $A(z) = A_0 e^{i\beta z}$, where $\beta = (k_0/2\sqrt{\epsilon_{\mathrm{b}}})\left\{\mathrm{Re}\left[\epsilon_{\mathrm{eff}}\left(|A_0|^2\right)\right] - \epsilon_{\mathrm{b}}\right\}$ and the amplitude A_0 is fixed by the condition $\mathrm{Im}[\epsilon_{\mathrm{eff}}\left(|A_0|^2\right)] = 0$, which is numerically solved through the Newton-Raphson method. We find a sub-critical bifurcation of extended nonlinear modes from the trivial vacuum $A_0 = 0$ and identify three types of modes: Type I and II coexist in the bi-stable sub-critical domain, while Type III exists only in the over-critical domain [see Fig. 3(a) in the main paper]. The stability of extended modes against small-amplitude perturbing waves with amplitude δA and wave-vector q is evaluated by setting

$$A = \left[A_0 + \delta A_1 e^{(\gamma + i\Upsilon)z + iqx} + \delta A_2^* e^{(\gamma - i\Upsilon)z - iqx}\right] e^{i\beta z},$$

where γ represents the instability growth rate and Υ is a propagation constant shift. Inserting this expression in Eq. (1) of the main paper, and linearizing with respect to the small-amplitudes $\delta A_1, \delta A_2$, we find a linear homogeneous algebraic system of equations, whose complex eigenvalues $\gamma + i\Upsilon$ are calculated numerically for every wave-vector q. Positive/negative growth rates γ indicate instability/stability against small-amplitude perturbations. We find that

Type I modes are always unstable, while Type II and III modes are unstable only for a finite range of q [see Fig. S1, where we plot the maximum instability growth coefficient γ against q]. Besides, Type II/III extended modes exist on top of a stable/unstable background $A_0 = 0$, respectively. Thus, nonlinear dynamics in sub-critical/over-critical domains leads to qualitatively different phenomena [see Figs. 3(c),(d) in the main paper].

Localized nonlinear modes are calculated by setting the ansatz $A(x,z) = A_0(x)e^{i\beta z}$ in Eq. (1) of the main paper. The ensuing differential equation for $A_0(x)$ is transformed into a nonlinear system of algebraic equations by discretizing the spatial variable $x = x_m$ and the second order derivative $\partial_x^2 A(x) = [A(x_{m-1}) - 2A(x_m) + A(x_{m+1})]/(x_m - x_{m-1})^2$ with $m = 1, 2, .., M$, and by applying homogeneous boundary conditions $A(x_1) = A(x_M) = 0$. This nonlinear system of algebraic equations is then numerically solved through the Newton-Raphson method. In the context of dissipative systems, these kinds of localized nonlinear modes are commonly named dissipative solitons (DSs) [6], as they involve an internal power flow enabling stationary propagation. We also find a sub-critical bifurcation from the trivial vacuum $A_0(x) = 0$ for these localized modes and identify three types of them: DS1 and DS2 coexist in the bi-stable sub-critical domain, while DS3 exists only in the over-critical domain [see Fig. 4(a) in the main paper, where we plot their maximum intensity $I_{\max} = (1/2)\epsilon_0 c \max|A_0(x)|^2$ and their width $w = 2[\int_{-\infty}^{+\infty} x^2|A_0(x)|^2dx/\int_{-\infty}^{+\infty}|A_0(x)|^2dx]^{1/2}$ against g_0 for fixed graphene flake density $N = 10^3\ \mu\text{m}^{-3}$]. Intensity profiles of DS1, DS2, and DS3 modes are plotted in Fig. S**??**(a), while their x-dependent phase $\phi = \text{atan}[\text{Im}A_0(x)/\text{Re}A_0(x)]$ is shown in Fig. S**??**(b). Interestingly, owing to the transverse inhomogeneous phase, for every localized mode there is a peculiar internal power flow enabling stationary propagation within an intensity-dependent absorption/amplification environment [see Fig. S**??**(d)].

The stability of localized modes is studied in propagation. All propagation plots have been obtained by solving Eq. (1) of the main paper through the split-step fast-Fourier-transform method embedding a fourth-order Runge Kutta routine.

[1] K. L. Ishikawa, *Phys. Rev. B* **82**, 201402(R) (2010).
[2] K. L. Ishikawa, *New J. of Phys.* **15**, 055021 (2013).
[3] B. Nithyaja, H. Misha, P. Radhakrishnan, and V. P. N. Nampoor, *Appl. Phys. Lett.* **109**, 023110 (2011).
[4] M. A. Noginov *et al.*, *Phys. Rev. Lett.* **101**, 226806 (2008).
[5] F. J. García de Abajo, *ACS Photon.* **1**, 135 - 152 (2014).
[6] P. Grelu and N. Akhmediev, *Nat. Photon* **6**, 84 - 92 (2012).